Article:
Pitt, K. and Hounslow, M.J. (2015) Aggregation of growing crystals in suspension: III. Accounting for adhesion and repulsion. Chemical Engineering Science, 133. 148 - 156. ISSN 0009-2509

https://doi.org/10.1010/j.ces.2014.12.055

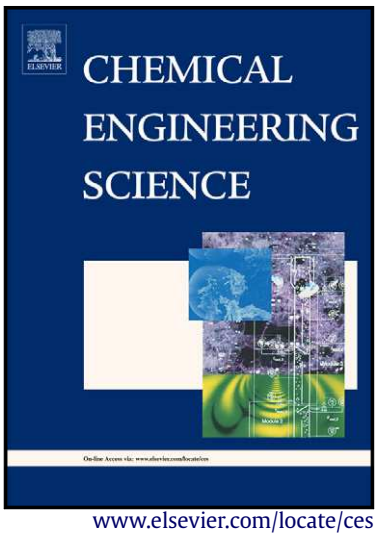

Aggregation of growing crystals in suspension: IIi. accounting for adhesion and repulsion

K. Pitt, M.J. Hounslow

PII: S0009-2509(14)00774-X
DOI: http://dx.doi.org/10.1016/j.ces.2014.12.055
Reference: CES12084

To appear in: *Chemical Engineering Science*

Received date: 19 August 2014
Revised date: 30 November 2014
Accepted date: 20 December 2014

Cite this article as: K. Pitt, M.J. Hounslow, Aggregation of growing crystals in suspension: IIi. accounting for adhesion and repulsion, *Chemical Engineering Science,* http://dx.doi.org/10.1016/j.ces.2014.12.055

AGGREGATION OF GROWING CRYSTALS IN SUSPENSION: III. ACCOUNTING FOR ADHESION AND REPULSION

K. Pitt[2], M.J. Hounslow[1,2]

Abstract

In this paper we modify our previously published model describing the aggregation behaviour of crystals growing in suspensions. That model considered aggregation only in terms of cementing, i.e the growth of a neck between colliding particles.

In this current work, we introduce into our model the case of aggregation of growing crystals in the presence of inter-particle forces. Here we postulate that aggregation may be augmented by adhesion between the colliding particles, or diminished by repulsion of particles. In the new model we characterise the adhesive or repulsive force by a surface energy acting along a linear contact and subsequently define an *adhesion* Mumtaz number, M_A. In the case of simultaneous cementing and adhesion the Mumtaz number is simply the sum of the separate cementing and adhesion numbers.

In this work, two crystallographic forms of calcium oxalate monohydrate (COM) and one form of calcite under both low and high ionic strength conditions were studied. Calcite crystals were found to evidence adhesion between the colliding particles, both a high and low ionic strength. Furthermore, the ionic strength also influenced the cementing parameter. The different forms of COM exhibited both different cementing and inter-particle behaviour. These effects were attributed to differences between the

[1] Corresponding Author: email m.j.hounslow@sheffield.ac.uk

[2] Department of Chemical and Biological Engineering, The University of Sheffield, Sheffield S1 3JD, UK

systems at the nano-scale and that aggregation behaviour depends on the anisotropic nature of growing crystals.

Keywords

Aggregation, Colloidal phenomena, Crystallisation, Aggregation Efficiency, Calcium oxalate monohydrate, Calcite

Introduction

When crystals grow in a suspension they will from time to time collide as a consequence of their relative motion and if the contact between them is sufficiently strong, aggregation of the crystals will occur. The fraction of such collisions that result in an aggregation event, we term the aggregation efficiency.

In Part I of this series (Hounslow et al., 2013) we considered from first principles the case where the strength of the contact arose from the growth of a neck between the colliding particles and showed that in that case the efficiency would depend locally on a dimensionless strength we term the Mumtaz number, M.

In Part II of this series (Pitt and Hounslow, 2014) we described the design and operation of a Poiseuille Flow Crystalliser (PFC). This novel technique allows the interrogation of the effect of hydrodynamic and physico-chemical conditions on the aggregation of particles in suspension. The PFC operates as a differential reactor where changes in particle size distributions can be used to yield a quantitative description of aggregation.

Using the PFC we can also determine a value for the material property controlling aggregation – the product of the yield strength of the material, σ_y, and a geometric factor with dimensions of length, L^* (Pitt and Hounslow, 2014).

We introduced a critical aggregate size, D, as the particle size that at the average shear rate has a Mumtaz number of $M = 1$, so disruptive shear forces are in balance with the strength of the growing neck. Here, we obtained values for D for calcium oxalate monohydrate (COM) by fitting the change in size distributions in the PFC. For COM, the values of D^2 were found to be directly proportional to the ratio of crystal growth to the flow rate squared, and we found no evidence of attractive or repulsive inter-particle forces active in promoting or retarding aggregation in this COM system (Pitt and Hounslow, 2014).

In this paper, we allow that the strength might be augmented by adhesion or reduced by repulsion between the colliding particles. Studies of adhesion between small particles are ubiquitous in the colloids literature, but much rarer in studies of growing crystals, An exception to this is the work of (Alander and Rasmuson, 2005) who

conclude that growth alone is not sufficient to account for agglomeration between growing crystals of paracetamol in acetone/water solutions. We refer to the process of growing a neck as cementing and the net adhesion or repulsion as simply adhesion. For this study, two different materials were used; calcium oxalate monohydrate (COM) and calcite.

Two different types of COM crystals were considered, each presenting different crystallographic identities. The study of calcite involved operating the PFC under both low and high ionic strength conditions.

Theory

Our intention here is to understand behaviour of growing crystals and expect, therefore, cementing to be present if not dominant. However the analysis is simpler if we first consider adhesion in isolation before considering how to treat simultaneous cementing and adhesion. In what follows, we assume that failure is always a consequence of simple tension; that is the normal component of the disruptive force exceeds a critical value, often expressed as a stress.

Adhesion Only

Following the analysis developed in Part I we consider whether a newly formed doublet of particles can withstand the periodic hydrodynamic drag experienced as a consequence of fluid shear. We characterise the adhesive or repulsive force by a surface energy (per unit area, so force per unit length), Γ, acting along a linear contact of length, L. If the force is attractive, Γ is positive. If it is repulsive, Γ is negative. A contact will rupture if the normal tensile force exceeds an adhesive force:

$$F_N - L\Gamma > 0 \tag{1}$$

The normal force varies over time with the relative position of the doublet to the shear field, as described by a pair of Euler angles θ and ϕ. The rupture criterion is

$$L\Gamma = \frac{\pi}{8} d_I d_{II} \mu\dot{\gamma} \sin^2\theta \sin 2\phi \tag{2}$$

or

$$\frac{L\Gamma}{\dot{\gamma} d_I d_{II} \mu} = \frac{\pi}{8} \sin^2 \theta \sin 2\phi \tag{3}$$

where d_I *and* d_{II} are the particle diameters, μ is the dynamic viscosity of the solution and $\dot{\gamma}$ is the local shear rate.

The left hand side of eq (3) defines an *adhesion* Mumtaz number, M_A, based on a geometric mean size. In general

$$M_A = \frac{L\Gamma}{\dot{\gamma} d^2 \mu} \tag{4}$$

Using the methodology developed in Part I, for any value of M_A it is possible to determine the collision orientations that satisfy the rupture criterion and so determine which initial collision orientations give rise to an aggregate and which do not. In Figure 1, a series of collision cross sections are shown for various adhesion Mumtaz numbers and ratios of particle sizes:

$$\lambda = d_I / d_{II} \tag{5}$$

The results shown here contrast with those for cementing shown in Figure 9 of Part I. When only adhesion is available to resist the shear force, the collisions must also lie near the poles (ie where the vertical axis crosses the collision circle) of Figure 1 in Part I. In the presence of cementing, those collisions that originate near the centre of the cross-section have sufficient time to grow a strong neck of new material.

λ = 1

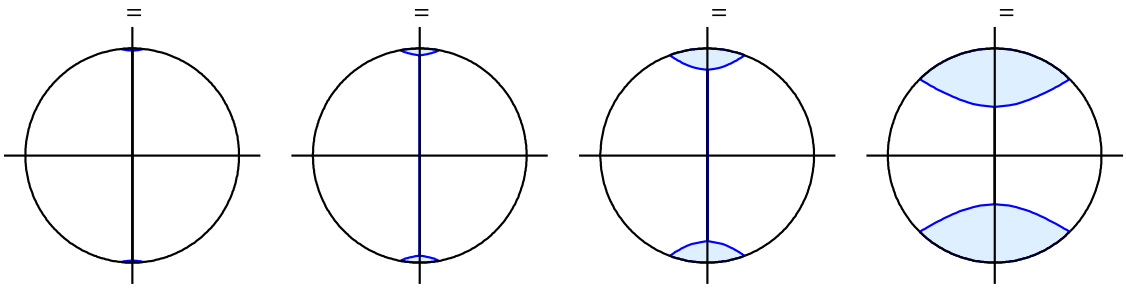

λ = 3

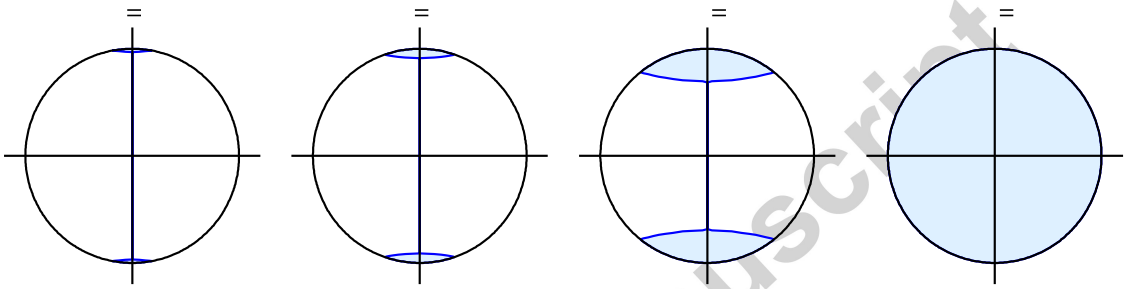

λ = 10

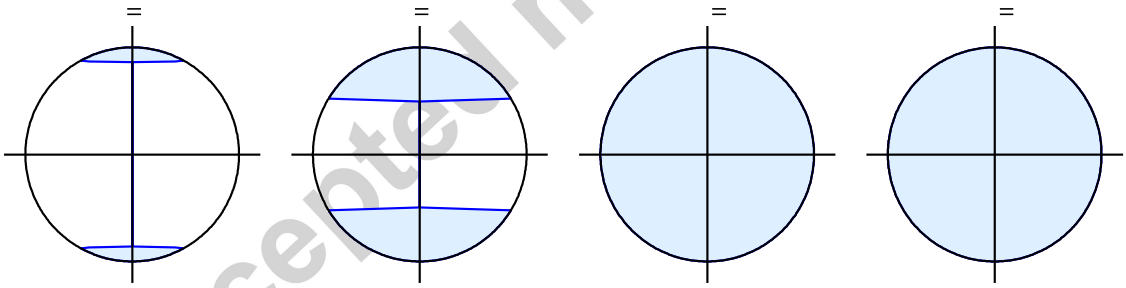

Figure 1. Successful collision orientations for a range of size ratios and adhesion Mumtaz numbers defined in eq (4) using the geometric mean size. Any orientation in the shaded area gives a stable aggregate.

Following the methodology developed in Part I of averaging over all collision orientations, and then developing an equivalent diameter:

$$d_{eq} = q\sqrt{d_I d_{II}} \tag{6}$$

we can calculated the collision efficiency as shown in Figure 2. The size correction factor (q) used in that figure is found to be essentially identical to that shown in Figure 11 of Part I.

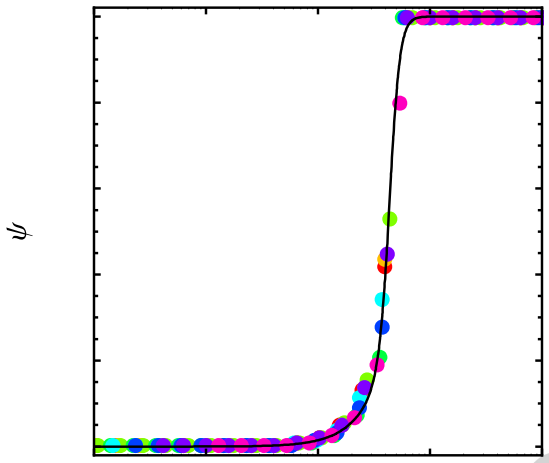

Figure 2. Efficiency for adhesion only at different size ratios, λ, using an adhesion Mumtaz number based on equivalent diameter. The line shown corresponds to the parameters (m and n) of Table 1. The colour coding is as Figure 10 of Part I.

Averaging for the PFC

The result shown in Figure 2 corresponds to efficiencies at a point in space, since M_A varies with shear rate and shear rate is normally expected to vary with position. We wish to apply these results to data from the PFC so following the development of Part II the appropriate average efficiency $\overline{\overline{\psi}}$ can be calculated once the average Mumtaz number is known

$$\overline{\overline{M}}_A = \frac{\Gamma L}{\overline{\overline{\dot{\gamma}}} d_{eq}^2 \mu} \tag{7}$$

Eq 19 of Part II gives

$$\begin{aligned}\bar{\bar{\psi}} &= \frac{3}{R^3}\int_0^R r^2\psi(r)\,dr \\ &= \frac{8\bar{\bar{M}}_A^3}{9}\int_{\frac{2}{3}\bar{\bar{M}}_A}^{\infty}\psi(M)\,M^{-4}\,dM\end{aligned} \tag{8}$$

which can be applied numerically to the result of Figure 2 giving the result of Figure 3 and the parameters in Table 1.

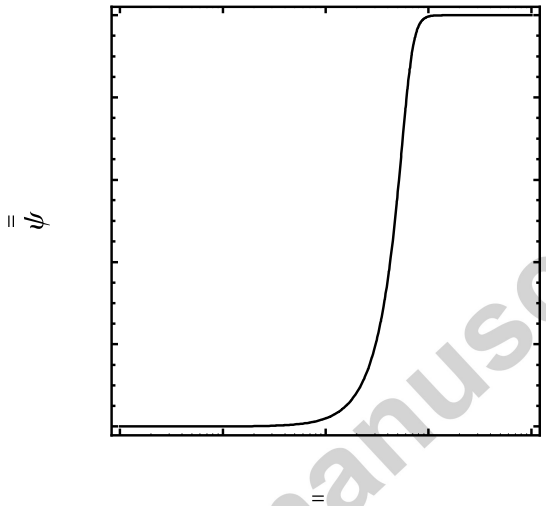

Figure 3. Average efficiency in the PFC for adhesion only.

Table 1. Parameters for the dependence of efficiency on M using eq 41 or 42 of Part I

Point values or PFC averaged	Curve fit to $\psi(M)$				Properties of ψ□□□ or $\bar{\bar{\psi}}\left(\bar{\bar{M}}\right)$	
	a	α	m	n	location $\bar{M}_g$	spread σ_g
point: ψ□□□	4.206	0.738	2	10	3.89	1.47
averaged: $\bar{\bar{\psi}}\left(\bar{\bar{M}}\right)$	4.835	0.346	2	10	4.18	1.66

Comparing these results – for adhesion only – with those of Table 1 of Part II for cementing only shows that

- For low efficiencies, ψ scales with a similar power of the relevant Mumtaz number, m = 2 or 1.5
- The transition to ψ = 1 is more abrupt under adhesion
- Under adhesion the efficiency curve has less spread and is located at larger values of Mumtaz number.

So while failure under adhesion gives a different efficiency curve to that under cementing, the differences are modest.

Simultaneous adhesion and cementing

The analysis of Part I was repeated to include strength induced by adhesion and cementing. The result is a function of efficiency, ψ, in three dimensions: two Mumtaz numbers – M_C and M_A – and the size ratio, λ. Various methods of reducing the dimensionality of the function were developed and all worked well when applied to PFC data. A significantly simpler and easier way to apply the results was also developed using a scaling analysis. That result is now presented.

When we introduced the Mumtaz number we did so on the basis of a scaling analysis that postulated that the strength of the neck should go as

$$\text{strength} \sim \text{rate of growth of neck} \times \text{time for growth of neck} \times \text{length of neck} \times \text{yield strength}$$
$$\sim G \times \frac{1}{\dot{\gamma}} \times L^* \times \sigma_y$$

while the disruptive forces go as

$$\text{disruptive force} \sim \dot{\gamma} \mu d^2$$

So

$$M = \frac{\text{strength}}{\text{disruptive force}} = \frac{G \times \frac{1}{\dot{\gamma}} \times L^* \times \sigma_y}{\dot{\gamma} \mu d^2}$$

If we now allow that the strength is enhanced by adhesion so that

$$\text{strength} \sim \frac{GL^*\sigma_y}{\dot{\gamma}} + L\Gamma$$

the Mumtaz number becomes

$$M_{\text{C+A}} = \frac{GL^*\sigma_y}{\dot{\gamma}^2\mu d^2} + \frac{L\Gamma}{\dot{\gamma}\mu d^2} = M_{\text{C}} + M_{\text{A}} \tag{9}$$

In other words, the Mumtaz number for simultaneous cementing and adhesion is simply the sum of the separate cementing and adhesion numbers.

In Part II it was convenient to describe a critical aggregate size that we should now term the critical cementing particle size

$$D_{\text{C}}^2 = \frac{GL^*\sigma_y}{\dot{\gamma}^2\mu} \tag{10}$$

So that as a function of particle size the cementing Mumtaz number can be written

$$M_{\text{C}} = \left(D_{\text{C}}/d\right)^2 \tag{11}$$

By analogy a critical adhesion particle size can be defined

$$D_{\text{A}}\left|D_{\text{A}}\right| = \frac{L\Gamma}{\dot{\gamma}\mu} \tag{12}$$

We take care to write the left hand side of eq (12) in this form to allow that both Γ and D_{A} can be negative.

From eq (9) we can then also write

$$D_{\text{C+A}}^2 = D_{\text{C}}^2 + D_{\text{A}}\left|D_{\text{A}}\right| \tag{13}$$

This scaling analysis indicates that eq (9) can be used to calculate the effective Mumtaz number; it does not identify how efficiency should depend on that value. Two functions, ψ_{C} and ψ_{A}, are available in the limits $M_C >> M_{\text{A}}$ and $M_{\text{A}} >> M_{\text{C}}$. However, since the purpose of this work is to understand aggregation of growing crystals (and so

cementing is likely to be more important than adhesion) and that the two functions are not very different in shape, in this work we use ψ_C, i.e.;

$$\psi_{C+A}\left(M_{C+A}\right)=\psi_C\left(M_{C+A}\right)=\psi_C\left(M_C+M_A\right) \tag{14}$$

Application to the PFC

Eqs (9) to (14) can be applied directly with the shear rate, $\dot{\gamma}$, replaced by the in-situ average, $\bar{\dot{\gamma}}$, the particle size, d, by the geometric mean of the colliding particles, $\bar{d}_g$, and efficiency and Mumtaz number replaced by their apparent averages, $\bar{\bar{\psi}}$ and $\bar{\bar{M}}$.

The approach taken in Part II of fitting a value for the critical aggregate size to measured values of $\Delta n\left(d\right)$ can still be used. So for any one experiment a value of D is obtained.

In Part II, eq 35, in the absence of adhesion we showed that in theory and in practice D^2 is directly proportional to the ratio of growth rate to flow rate squared $\frac{G}{Q^2}$. In the present work we obtain:

$$D_{C+A}^2=\frac{L^*\sigma_y}{\mu}\left(\frac{3\pi R^3}{8}\right)^2\frac{G}{Q^2}+\frac{L\Gamma}{\mu}\frac{3\pi R^3}{8}\frac{1}{Q} \tag{15}$$

So, for a fixed flowrate, a plot of D^2 against G is a straight line with a slope related to the unknown cementing parameters, $L^*\sigma_Y$, and an intercept related to the adhesion parameters $L\Gamma$. In the absence of adhesion the intercept is zero and so the line passes through the origin. If an attractive force is present the intercept is positive and if repulsion is active, the intercept is negative.

In cases where the flow rate is not fixed Eq (15) can also be used via simple *multiple* linear regression, treating $\frac{G}{Q^2}$ and $\frac{1}{Q}$ as independent variables, and D^2 as a dependent variable, to determine the unknown parameters, $L^*\sigma_Y$ and $L\Gamma$. An equivalent result can be obtained by multiplying both sides of eq (15) by Q to give

$$QD_{C+A}^2 = \frac{L^* \sigma_y}{\mu}\left(\frac{3\pi R^3}{8}\right)^2 \frac{G}{Q} + \frac{L\Gamma}{\mu}\frac{3\pi R^3}{8} \quad (16)$$

Which is to say, a plot of QD^2 against $\frac{G}{Q}$ has a slope related to the influence of cementing and an intercept that is influenced by adhesion.

Experimental

Poiseuille Flow Crystalliser

In this paper, we describe how the characteristics of Poiseuille flow can be exploited in a study of the aggregation of both calcium oxalate monohydrate (COM) and calcite using the Poiseuille flow crystalliser (PFC).

The design and operation of the PFC are described in detail in Part II of this series. Crystal size distributions were measured using an Accusizer 780 optical particle sizer (PSS.NICOMP Particle Sizing Systems, Santa Barbara, US), which is also detailed in Part II.

Materials

All chemicals used in the preparation of seed suspensions and PFC solutions were of analytical grade. The water used was distilled, deionised and filtered using an Elga Classic DI Mk2 purification system with a 0.2μm filter.

(a) Calcium oxalate monohydrate (COM) studies

Seed suspensions

Two different types of seed suspension were prepared; (i) seed suspensions consisting of crystallographically poorly-defined COM crystals, referred to as *rounded* COM, and (ii) seed suspensions of crystallographically well-defined COM crystals.

The preparation of these seed suspensions is detailed fully in Part II of this series. The crystallographic identity of these crystals is described in (Pitt et al., 2012) as is their growth rate.

Solutions for PFC

The preparation of saturated and metastable solutions for use in the PFC is described in detail in Part II.

(b) Calcite studies

Seed suspensions

Seed suspensions were prepared by wet grinding 1g of commercially supplied calcite (Fisher Scientific) in a mortar and then suspended in a saturated solution of calcite (1 litre). This seed suspension was stored at 21°C in a seed reservoir at the top of the PFC and stirrer using an overhead stirrer. Suspensions were aged for a minimum of one week prior to use.

Solutions for PFC

Two types of solutions were employed: metastable (supersaturated) and saturated.

Saturated solutions were prepared by adding solid calcite (Fisher Scientific) to pure water, magnetically stirred for a minimum of 24 hrs and filtered using 0.2μm pore size cellulose nitrate membrane filter papers (Whatmann, UK).

A range of metastable solutions were prepared having initial supersaturations ranging from S-1 = 1.41 – 8.60, where the relative supersaturation is defined as:

$$S = \sqrt{\frac{a_{Ca^{2+}} a_{CO_3^{2-}}}{K_{sp}}} \tag{17}$$

Where a is the ionic activity of the free ions, and K_{sp} is the thermodynamic solubility product = 1.25×10^{-9} at 21°C.

Growth rates for calcite calculated during previous studies have been shown to follow a parabolic rate law which depends on the supersaturation (Collier and Hounslow, 1999; Kazmierczak et al., 1982; Nancollas and Reddy, 1971; Nielsen and Toft, 1984; Tai and Chen, 1995) have shown from measurements of size distributions during batch crystallisation studies over a wide range of conditions that the linear rate of crystal growth is given by $G = k_g (S - 1)^2$, where $k_g = 1.28 \times 10^{-10}$ ms^{-1}.

In these solutions, the calcium ions are provided by $Ca(NO_3)_2$ and the carbonate ions by $NaHCO_3$. The final pH of the solution was adjusted to 9.6 by the addition of a few drops of NaOH. The resulting solutions had ionic strengths ranging from 0.0014 – 0.0069 M

In addition to the above experiments carried out at a relatively low ionic strength (i.e. using pure water to prepare the solutions), experiments were also carried out at relatively high ionic strengths (ranging from 0.1353 – 0.1409M) using a background electrolyte. KNO_3 was selected as the background electrolyte as it is reported potassium and nitrate ions have no effect on calcite growth and habit (Collier, 1997; Didymus et al., 1983; Sohnel and Mullin, 1982). A range of metastable solutions were prepared having initial supersaturations ranging from S-1 = 0.31 – 5.18.

Methods

For all COM and calcite studies, saturated solutions were fed to the PFC. The seed suspensions were subsequently introduced into the PFC via a peristaltic pump and the flow rate adjusted to the desired value. Crystal size distributions in saturated solution were then measured by the Accusiser and referred to as 'inlet' distributions. The solution feed was then changed from saturated solution to metastable solution and again, the crystal size distribution taken. These are referred to as 'outlet' distributions.

A more detailed account of the PFC method is given in Part II.

The range of operating conditions for each system and each of the four series of experiments is given in Table 2.

Table 2. Range of conditions for each of three series of experiments for each system. Rounded COM values taken from Part II.

System	Series name	Supersaturation $S-1$	Flow rate Q (ml min^{-1})	Seeds loading w_0 (kg m^{-3})
Rounded COM	"S"	1.65 – 3.10	0.75	0.42 – 0.58
	"Q"	2.68	0.5 – 1.0	0.41 – 0.53
	"w_0"	2.68	0.75	0.30 – 0.90
Well-defined COM	"S"	1.65 – 3.10	0.75	0.43 – 0.56
	"Q"	2.68	0.58 – 1.0	0.55 – 0.63
	"w_0"	2.68	0.75	0.21 – 0.64
Calcite with KNO_3	"S"	0.31 – 5.18	0.75	0.06 – 0.13
	"Q"	4.01	0.5 – 1.0	0.07 – 0.11
	"w_0"	4.01	0.75	0.06 – 0.14
Calcite without KNO_3	"S"	1.41 – 8.60	0.75	0.13 – 0.20
	"Q"	7.02	0.67 – 1.0	0.07 – 0.10
	"w_0"	7.02	0.75	0.09 – 0.16

Results

We fitted the simple tension model of Part I to data collected using the PFC according to the method of Part II. For each experiment a single parameter, the critical aggregate size, D, is fitted to the difference between the inlet and outlet size distributions of the PFC. Following the analysis leading to equation (15) we treat the observed value of D as the combined cementing and adhesion value D_{C+A}.

In Figure 4, D^2 is plotted against growth rate, in the style of eq (15) for the "*S*" datasets; that is for varying supersaturation and fixed flow rates. It is apparent that each of these sets is well-described by a straight line but in no case does the line pass through the origin. For well-defined COM the *y*-axis intercept is negative – indicating repulsion - while for both set of Calcite data the intercept is positive indicating adhesion. This is in contrast to rounded COM reported in Part II, where the line intercepts the origin, indicating no adhesion or repulsion.

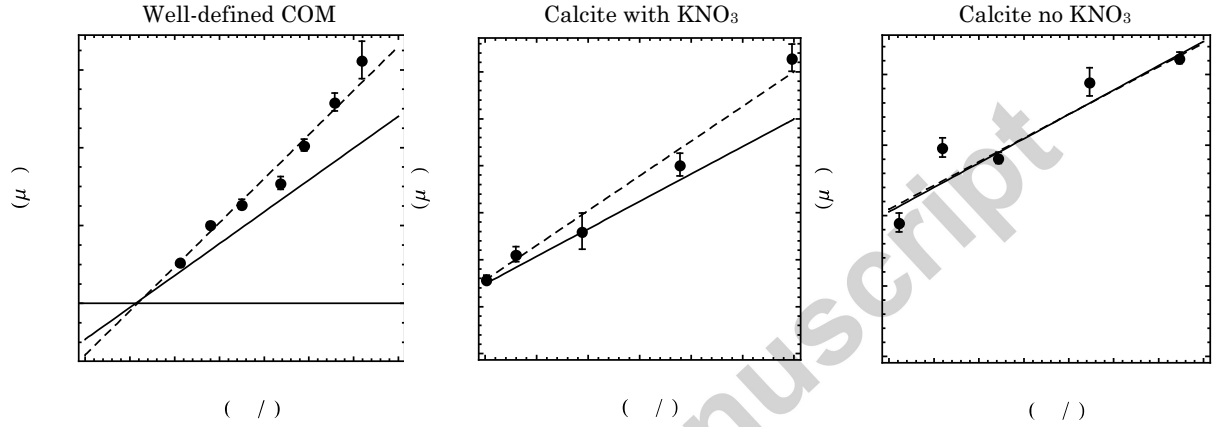

Figure 4. Critical aggregate size as a function of growth rate for fixed PFC flowrate. While well-defined COM shows a negative *y*-axis intercept – indicating repulsion – Calcite shows a positive intercept indicating attraction. The dashed lines are fitted to these data, the solid lines correspond to eq (15) and the parameters of Table 3.

In Figure 5 the data for the three systems presented here (well-defined COM, Calcite with and without KNO_3) and that presented in Part II are plotted according to the style of eq (16). The straight lines shown correspond to that equation and allow the two kinetic parameters, $L^*\sigma_Y$ and $L\Gamma$, given in Table 3 to be determined. The shaded regions show the 95% confidence interval for the model prediction – demonstration that the intercepts and slopes are readily determined.

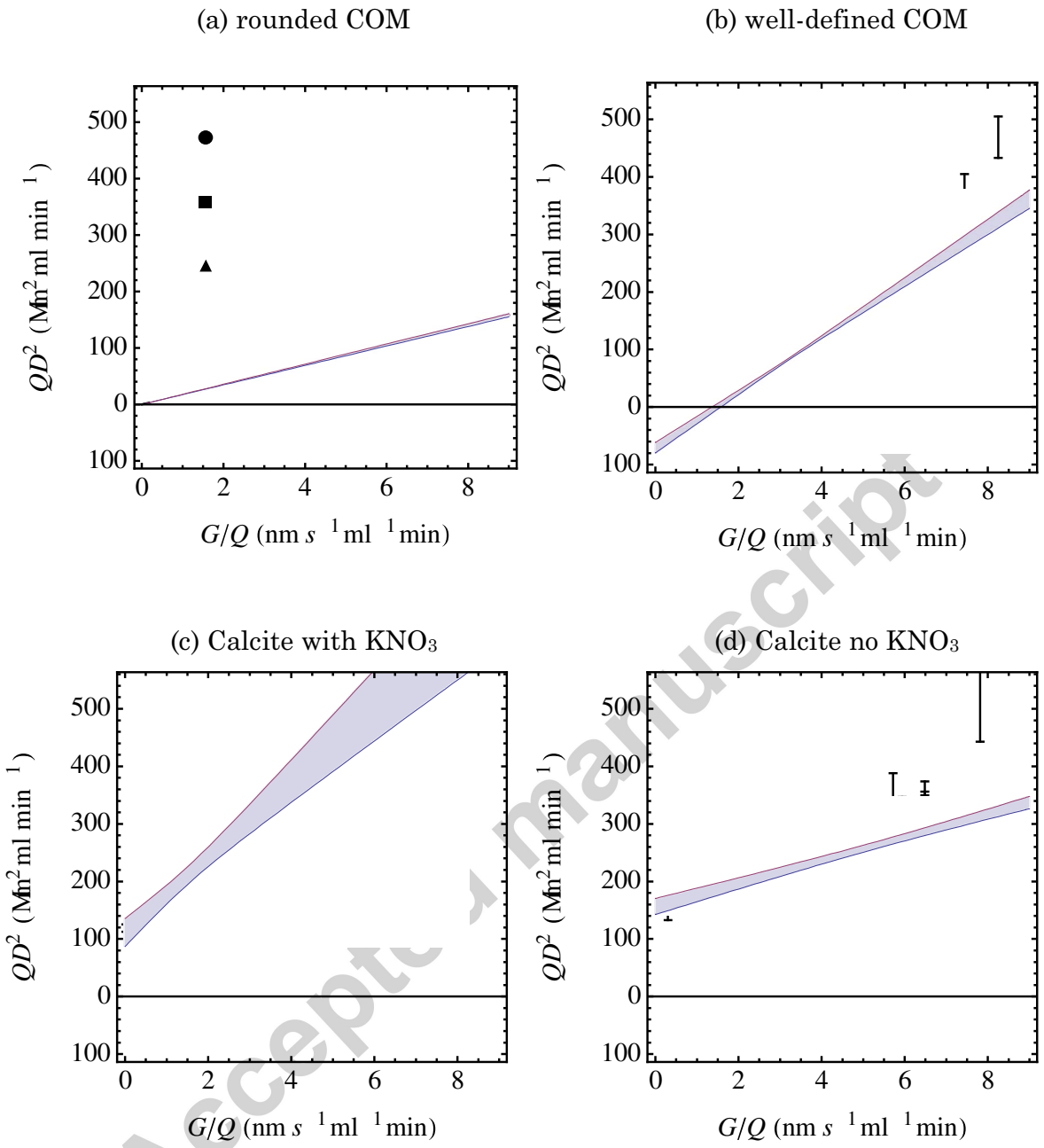

Figure 5. Kinetic plots according to eq (16) in which the *y* intercept indicates the contribution of adhesion (positive) or repulsion (negative) and the slope the contribution of cementing to the efficiency of aggregation. The line corresponds to eq (16) and the parameters of Table 3. The shaded area is the 95% mean prediction interval.

It is apparent that

- Rounded COM gives an intercept of zero (so no adhesion is present, as concluded in Part II) and a low slope indicating a relatively low tendency to cement
- Well-defined COM shows a negative intercept – so repulsion is present – and an increased influence of cementing (compared to rounded COM)
- Both calcite systems show a positive axis intercept indicating roughly equivalent levels of adhesion
- Calcite in the presence of KNO_3 shows an increased influence of cementing

For all four systems shown in Figure 5 the dispersion in the data – as shown by error-bars of ± one standard deviation – is not explained by the uncertainty in the model. A numerical investigation revealed that the errors in the data would need to be underestimated by less than a factor of 2 for the discrepancy to be well within the bounds of acceptable probability. A simpler qualitative exploration is shown in the parity plots of Figure 6: the model captures most of the variation seen in D .

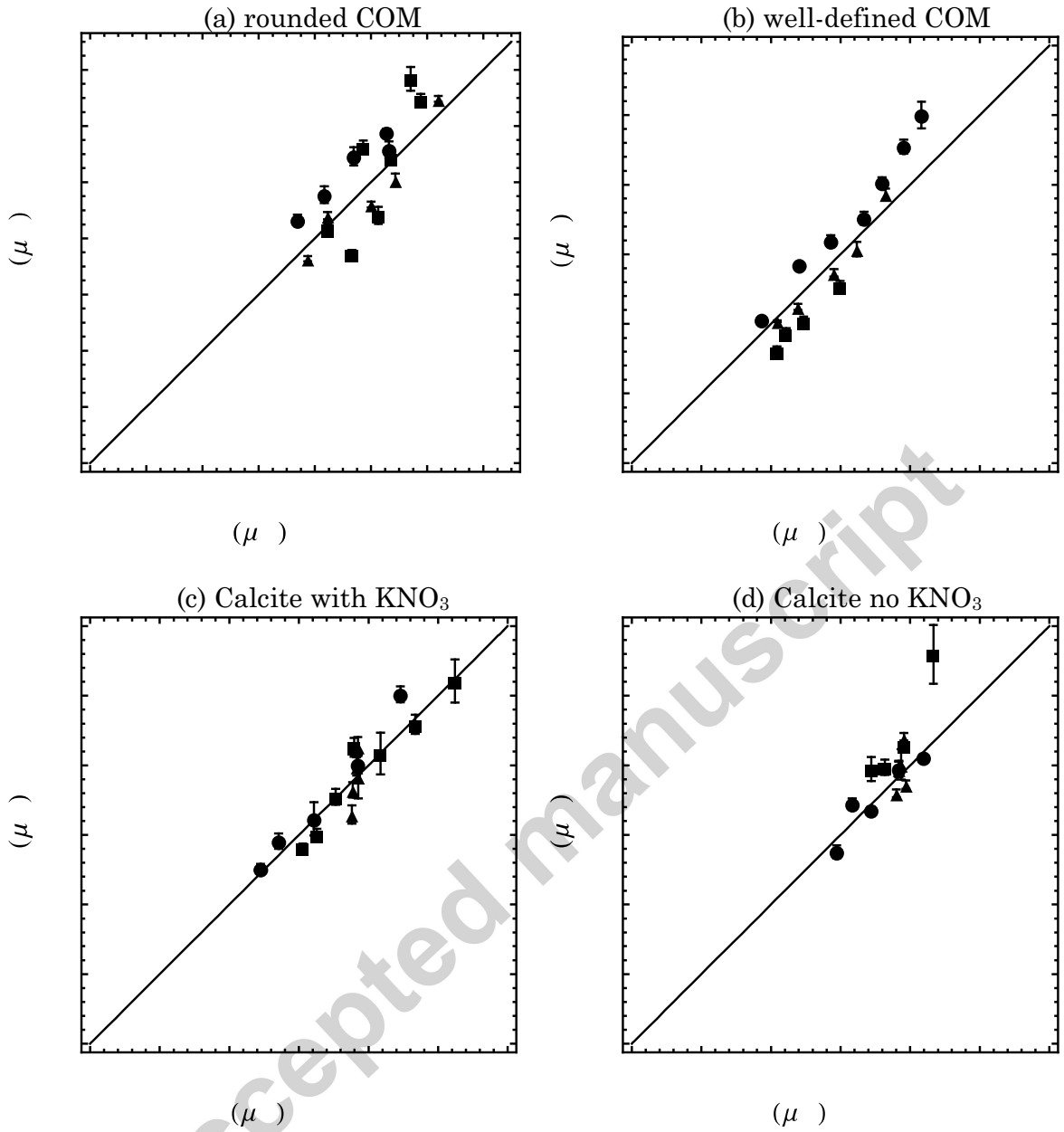

Figure 6. Parity plots for measured and predicted critical aggregate size. Most data lie within one standard error (shown by the error bars) of the prediction and nearly all within three. Legend as in Figure 5.

Table 3. Kinetic parameters deduced from Figure 5

System	$L^*\sigma_Y$ (Nm^{-1})	$L\Gamma \times 10^{11}$ (N)	R^2
Rounded COM	1.35±0.01	–	0.965
Well-defined COM	3.68±0.10	–1.95±0.11	0.971
Calcite with KNO_3	5.05±0.23	3.08±0.16	0.977
Calcite without KNO_3	1.54±0.08	4.35±0.18	0.986

Discussion

The theory culminating in eq (15) says that for a fixed flowrate the critical aggregate size squared should vary linearly with the growth rate, G, and that the slope is related to cementing kinetics and the intercept to attraction. For all four systems studied here that result is seen directly in Figure 4 and then in the more general form of eq (16) in Figure 5 for a broad range of experiments.

The slopes and intercepts of the lines in Figure 5 make it possible to estimate the kinetic parameters shown in Table 3.

We see that well-defined COM is significantly more prone to aggregate as a consequence of cementing than rounded COM, but that well-defined COM demonstrates repulsion. This former result is consistent with the observation in Pitt et al. (2012) that $L^*\sigma_Y$ is greater for well-defined seeds than for rounded. They attributed this observation to a difference in the growth rate of those crystal growth directions responsible for aggregation and those apparent macroscopically.

Calcite in the presence of KNO_3 evidences greater cementing than in its absence. Although the presence of K^+ is not known to affect the growth behaviour of calcite, K^+ has been reported to incorporate into interstitial sites in the calcite lattice during crystal growth, and Ca vacancies compensate for the excess charge of K^+ in calcite (Ishikawa and Ichikuni, 1984). It is possible that these defects at the nano-scale enhance cementing.

Calcite crystals were found to evidence adhesion, both at low and high ionic strength. Calcite particles are well-known to attract each other and agglomerate in aqueous solution. This is thought to be due to a low magnitude of zeta potential resulting in unstable suspensions (Eriksson et al., 2008; Tari and Ferreira, 1998).

It is interesting to note that well-defined COM evidences repulsive behaviour. This could be a consequence of the crystallographic nature of these crystals. Compared to rounded COM, these well-defined crystals express a relatively large proportion of surfaces with polar character (Millan, 2000Millan, 2000). These may be expected to equally promote attraction or repulsion of the crystals in solution. However, the attractive fraction may well be suppressed in the PFC system due to shear in the capillary, thereby leading to a net contribution of repulsive forces.

It is striking that all the explanations for the kinetic parameters in Table 3 rests on effects at the nano-scale. Either the density of linear defects – of a nano-size – changes or the crystallographic direction responsible for aggregation is only apparent at such length scales. So, at root, the aggregation behaviour depends on the anisotropic nature of growing crystals and on explanations that both reflect that anisotropy and, in anything but ideal systems, its variability on very small length scales.

For this reason, we believe that the approach first taken by Mumtaz and recently extended and applied in Part I – III of this series cannot reasonably be expected to be taken further. In both our theory and experiment we have characterised particle size by a single dimension of some microns and necessarily neglected the complex hierarchical structure of an aggregate, let alone the anisotropic character of individual crystals.

Inevitably, then, there is a substantial gap between a rigorous analysis based on surface science and that we have presented here. While we have been able to remove most of the averaging or smearing present because of varying particle size and distribution of shear rates, our representation of the surface of each particle can only be understood as an average. In that way our model is one of engineering approximation based on a plausible physical account that reduces quite complex observed behaviour to a pair of averaged materials properties – $L^{*}\sigma_{Y}$ and $L\Gamma$.

Conclusions

In Part I of this series we showed from first principles that when the rate of aggregation of growing crystals is controlled by their ability to cement together, that ability is described by an efficiency and that the efficiency should depend only on a dimensionless strength we term the Mumtaz number. Three open questions were articulated: which of several failure modes is active, what values does the materials property, $L^*\sigma_Y$, take, and how should point kinetics be averaged over a vessel?

In Part II we showed in a study of rounded particles of calcium oxalate monohydrate using a Poiseuille Flow Crystallizer that averaging was relatively straightforward, that failure of the cementing neck was apparently by simple tension and that values of $L^*\sigma_Y$ could readily be obtained by fitting a value for the critical aggregate size to PFC data. We also showed that as the crystal growth rate tended to zero so too did the critical aggregate size: that is crystal growth – or cementing – is required to overcome disruptive hydrodynamic forces in that system. By contrast, we have shown in the present paper that for COM in a different (well-defined) form, a finite rate of growth is needed before any aggregation is seen and that for calcite, aggregation will take place even in the absence of growth.

Acknowledgement

This work was funded in part by the UK Engineering and Physical Sciences Research Council under its grant reference EP/F008147/1

Nomenclature

a = parameter in eq 41 of Part I; activity
d = particle size (m)
d_g = geometric mean size of a pair of colliding particles (m)
D = critical aggregate particle size (m)
F_N = normal tensile force (N)
G = crystal growth rate (m s^{-1})
K_{sp} = solubility product (–)
L = length of the PFC capillary (m)
L^* = combined length and angle in the Mumtaz number (m)

m = parameter in eq 41 of Part I

M = Mumtaz number (–)

n = parameter in eq 41 of Part I

q = mean size correction factor (–)

Q = volumetric flow rate (m^3s^{-1})

r = radial coordinate (m)

r = a rate ($m^{-3}s^{-1}$)

R = capillary radius (m)

S = supersaturation ratio (–)

w_0 = feed seeds loading (kg m^{-3})

Greek letters

Γ = adhesive or repulsive surface energy (Nm^{-1})

α = parameter in eq 41 of Part I

$\dot{\gamma}$ = fluid shear rate (s^{-1})

Δ = a change (out – in)

λ = the ratio of size of two colliding particles

μ = viscosity (Pa s)

ψ = collision efficiency (–)

σ_g = spread of the efficiency curve given in eq 42 of Part I

σ_y = yield strength (Pa)

ϕ = Euler angle denoting the location of the initial point of contact with respect to the local fluid shear field

θ = Euler angle denoting the location of the initial point of contact with respect to the local fluid shear field

Subscripts

I, II = particles I and II of a colliding pair

A = refers to adhesion

C = refers to cementing

eq = equivalent

g = geometric mean

Other marks

$\bar{}$ = in-situ average

$\bar{\bar{}}$ = apparent average

Literature Cited

Alander, E.M., Rasmuson, A.C., 2005. Mechanisms of crystal agglomeration of paracetamol in acetone-water mixtures. Industrial & Engineering Chemistry Research 44, 5788-5794.

Collier, A.P., 1997. High resolution imaging of crystalline aggregates. PhD thesis, University of Cambridge.

Collier, A.P., Hounslow, M.J., 1999. Growth and aggregation rates for calcite and calcium oxalate monohydrate. Aiche Journal 45, 2298-2305.

Didymus, J.M., Oliver, P., Mann, S., DeVries, A.L., Hauschka, P.V., Westbroek, P., 1983. Influence of low-molecular-weight and macromolecular organic additives on the morphology of calcium carbonate. Journal of the Chemical Society Faraday Transactions 89, 2891-2900.

Eriksson, R., Merta, J., Rosenjolm, J.B., 2008. The calcite/water interface II. Effect of lattice ions on the charge properties and adsorption of sodium polyacrylate. Journal of Colloid and Interface Science 326, 396-402.

Hounslow, M., Wynn, E.J.W., Kubo, M., Pitt, K., 2013. Aggregation of growing crystals in suspension: I. Mumtaz revisited. . Chemical Engineering Science 101, 731-743.

Ishikawa, M., Ichikuni, M., 1984. Uptake of sodium amnd potassium by calcite. Chemical Geology 42, 137-146.

Kazmierczak, T.F., Tomson, M.B., Nancollas, G.H., 1982. Crystal growth of calcium carbonate. A controlled composition study. Journal of Physical Chemistry 86, 103-107.

Millan, A., 2000. Crystal growth shape of whewellite polymorphs: Influence of structure distortions on crystal shape. Crystal Growth & Design 1, 245-254.

Nancollas, G.H., Reddy, M.M., 1971. The crystallisation of calcium carbonate II. Calcite growth mechanism. Journal of Colloid and Interface Science 37.

Nielsen, A.E., Toft, J.M., 1984. Electrolyte crystal growth kinetics. Journal of Crystal Growth 67, 278-288.

Pitt, K., Hounslow, M., 2014. Aggregation of growing crystals in suspension: II. Poiseuille Flow Crystalliser. Chemical Engineering Science submitted.

Pitt, K., Mitchell, G.P., Ray, A., Heywood, B.R., Hounslow, M.J., 2012. Micro-mechanical model of calcium oxalate monohydrate aggregation in supersaturated solutions: Effect of crystal form and seed concentration. Journal of Crystal Growth 361, 176-188.

Sohnel, O., Mullin, J.W., 1982. Precipitation of calcium carbonate. Journal of Crystal Growth 60, 239-250.

Tai, C.Y., Chen, P.C., 1995. Nucleation, agglomeration and crystal morphology of calcium carbonate. AICHE J 41, 68-77.

Tari, G., Ferreira, J.M.F., 1998. Colloidal processing of calcium carbonate. Ceramics International 24, 527-532.

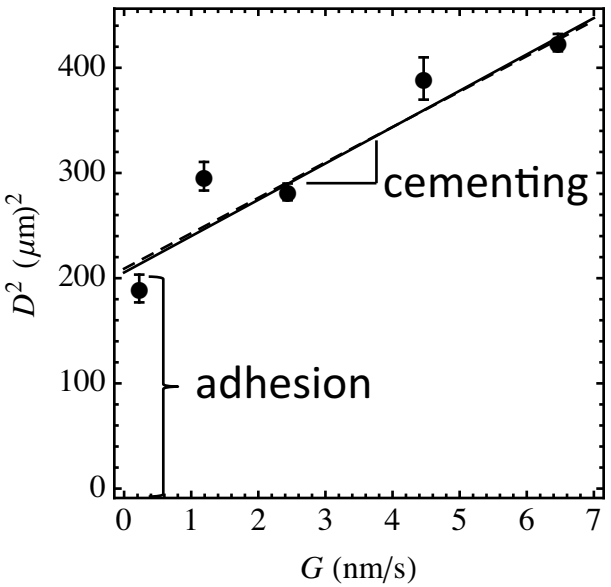

Highlights

- Our model for aggregation is extended to allow for adhesion and repulsion.
- We quantify the rate of aggregation and the contributions of cementing and adhesion
- Nano-scale properties of crystals influence both cementing and adhesion